Validation Study on External Wind Noise Prediction using OpenFOAM

*Mohamed Sukri Mat Ali**
Nur Haziqah Shaharuddin
Wind Engineering Laboratory,
Malaysia-Japan International Institute of Technology,
Universiti Teknologi Malaysia Kuala Lumpur,
54100 Kuala Lumpur, Malaysia
**sukri.kl@utm.my*

Jafirdaus Jalasabri
Anwar Mohd Sood
Compuatational Fluid Dynamics (CAE),
Vehicle Integration and Analysis,
PROTON Holdings Berhad,
40918 Shah Alam, Malaysia

Shuhaimi Mansor
Faculty of Mechanical Engineering,
Universiti Teknologi Malaysia Johor Bahru,
81310 Johor, Malaysia

ABSTRACT

Driven by the customer's demand for a low interior noise while keeping the cost of the car to a minimum, the direction for aerodynamic noise reduction is to mitigate its noise source generation. However, the aerodynamic noise generation is complex due to its turbulent nature. This paper presents a validation study in predicting the noise generation due to the turbulent flow near the A-pillar and it's estimated sound level if the sound source is transmitted inside the cabin through the side window glass. The case under study is a generic vehicle model, SAE type 4-fullback body, for its available data to be compared. The noise source is obtained from the numerical simulation using open source CFD packages, OpenFOAM and Curle's equation is used to estimate the sound propagation. The interior sound pressure level is then estimated by assuming sound transmission loss using the law of theoretical frequency for all ranges of noise frequency. A good

ISSN 1823- 5514, eISSN 2550-164X
Received for review: 2017-10-11
Accepted for publication: 2018-07-23
Published: 2018-11-30

agreement of the sound pressure level (SPL) between the current calculations and previous experimental measurements are obtained for frequency ranges between 200 Hz to 2000 Hz. The different in the other frequency ranges is mainly due to the invalid assumption when applying the law of theoretical frequency at these typical frequency ranges.

Keywords: *OpenFOAM; Wind Noise; A-Pillar; SAE Fullback Body*

Nomenclatures

p	Hydrodynamic pressure (Pa).
p'	Sound pressure (Pa).
U_∞	Free stream velocity (m/s)
k	Kinetic energy (m^2/s^2)
x	Observer position
y	Sound source position
n	Normal vector
C_o	Speed of sound (m/s)
D	Sound source length scale (m)
L	Total length of the A-pillar (m)
R	Sound transmission loss (dB)
Ma	Mach number (U_∞/C_o)

Greek Symbols

ω	Turbulent dissipation rate ($1/s^2$)
δ	Dirac delta function
λ	Sound wave length (m)
θ	Sound directivity (°)

Abbreviations

rms	Root mean square
SSL	Sound source level (dB)
SPL	Sound pressure level (dB)

Introduction

The noise emitted from a moving passenger car is a total contribution from three major noise sources. There are from the engine, tyres and free-stream flow over the body. At high speed (≥ 100km/h), aerodynamically generated noise can be the dominant noise source and its sound power increases with speed by V^6, but the other noise sources only increase between V^1 to V^3 [1]. Hucho [2] stated that when a car moving at 150 km/h with 5500 rpm engine

speed, 78.5 dB(A) from the total noise of 85 dB(A) that are measured at the driver's ear, is generated by the aerodynamic noise. Therefore, it is important to control the aerodynamically generated sound so that the total noise generated on the car can be reduced.

The interaction between the highly unsteady flows with the component body of the car induces fluctuating hydrodynamic pressure that is responsible for the emission of aerodynamic noise. The effectiveness of the noise propagates inwards the passenger compartment is strongly related to the magnitude of the noise sources. These noise sources can be from the turbulent boundary layer thickness (cardioid directivity with the intensity of $I \sim Ma^3$), Reynolds stress fluctuating (quadrupole directivity with the intensity of $I \sim Ma^8$) and aerodynamic force fluctuating (dipole directivity with the intensity of $I \sim Ma^6$) acting on the body.

In real life, info on the components of the car that generate significantly the aerodynamic noise is not well shared by the car manufacturers. One of the reason is that the technology for reducing aerodynamically generated noise is one of the key performances of a high-quality car. For a generic car model, an alliance of German car manufacturers has made an experimental sound measurement to localise the noise sources [3]. Using acoustic camera located 3.5 m from the car model, the noise sources are found to be originated dominantly from the front vertical support (A-pillar) and also the side view mirrors of the generic car model at a frequency in the range of 500 Hz to 10000 Hz. These noise sources become a major issue in driving comfort level as they are located very close to the front seats. Thus, the study on the aerodynamically generated sound from the interaction of flow with these car components (A-pillar and side view mirror) of a passenger car is important for the car manufacturers.

However, the prediction of aerodynamically generated sound is computationally time-consuming and experimentally expensive. Direct numerical simulation is the ideal solution to resolve all the time and length scales of turbulent flow that is responsible for the generation of the noise. But, it is limited by the very long time required to solve all the turbulent scales. Thus, it is not suitable for the industrial application. A hybrid approach, at which the noise source is obtained from the incompressible flow field seems more appropriate for the industrial application. The incompressible flow can be solved using appropriate turbulent model and the sound radiation is predicted using an acoustic analogy.

The main objective of this study is to validate the Unsteady Reynolds Averaged Navier-Stokes equations (URANS) for prediction of internal noise due to A-pillar vortex. Open source CFD package, OpenFOAM, is used to solve the governing equation and acoustics analogy that is based on Curle's equation is used to predict the sound pressure level inside the cabin. The validation is made by comparing the current numerical results with the experimental measurement by Hartmann et al. [3].

Problem Geometry

The problem geometry under investigation is an SAE type 4 model. It is a simplified car model where some small components of the cars are neglected in the design. For a validation purpose, the height and length are taken the same as the model being experimentally investigated by refs [3,4,5]. The dimension and geometry of the model are shown in figure 1. Further explanation of the model can be referred to in the author's previous paper [6].

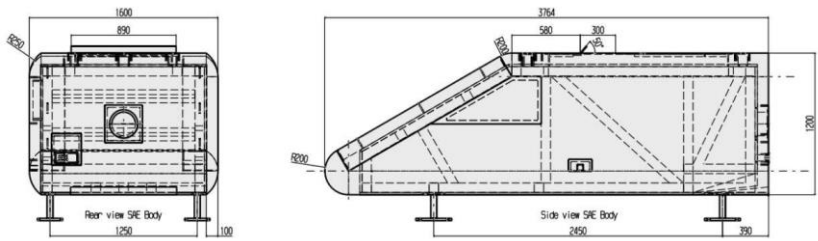

Figure 1 Schematic diagram of the SAE type 4 model [4].

Computational Setting

The numerical simulations are conducted using open source CFD package, OpenFOAM version 2.3.0. It is based on the finite volume method, where each of the control volumes is treated for its flow physical conservation using governing equations. The following subsection discusses the preparation of the control volume and the solutions used to solve the governing equations.

Computational Domain

The model is placed in the virtual wind tunnel (computational domain) as shown in Figure 2. To prevent the effect of the physical boundary of the tunnel, the computational domain is made large. The distances between the inlet, top and side of the tunnel from the model are the same, i.e., 10D, where $D = (\text{Frontal Area})^{1/2}$. The outlet is located at a longer distance, i.e., 20D from the model to allow the wake to dissipate naturally. The ground clearance is made the same as the experimental measurement of Hartmann et al. [3], i.e., 0.2 m, and two physical boundary conditions are used. Upstream of the model, slip boundary condition is used to eliminate the development of boundary layer on the upstream floor, while at downstream no-slip boundary condition is used to allow the effect of viscosity from the wake interacting with the downstream floor. In an effort to reduce the computational time, only half model is simulated, where a symmetry plane is used to numerically

consider the flow for the other half of the model. Table 1 listed the numerical boundary condition on the selected physical boundaries.

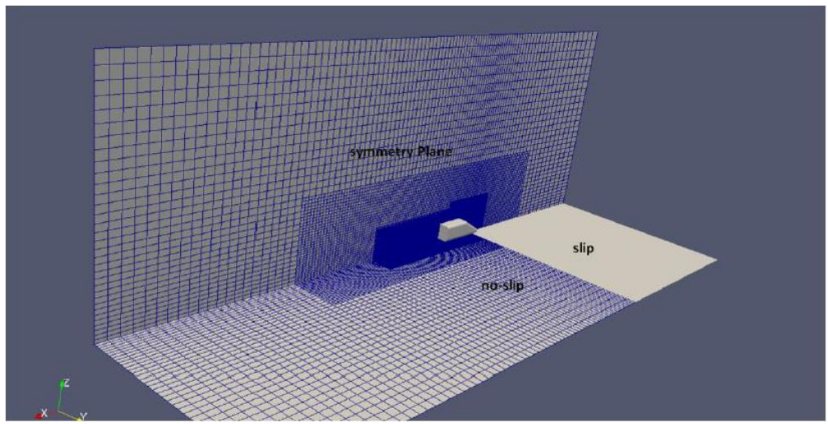

Figure 2 The computational domain. The total length of the computational domain is 33D

Table 1 The numerical boundary conditions. The numerical boundary condition for the upstream ground floor is a slip condition for all parameters

	Body	**Downstream floor**	**Side**	**Top**	**Inlet**	**Outlet**
p ***(kg/ms^2)***	Zero gradient					0
U ***(m/s)***	0		U_∞			Zero gradient
k ***(m^2/s^2)***	Wall function		$U_\infty^2 \times 10^{-6}$			Inlet Outlet
ω ***(1/s^2)***	Wall function		5 U_∞/33D			Zero gradient

To capture the small scale of eddies near the model, the grid is made from few refinement boxes. The smallest size is located at the front surface of the model where a layer of 0.0003 m thickness is constructed. At this region, the boundary layer and flow separation are expected to happen. At the downstream surface of the model, the layer of the mesh is made bigger, i.e., 0.0135 m of thickness. Then, a structured mesh with cell size average of ~0.04 m is constructed. Further away from the model, the cell size is two times bigger than the later. A total of 1.35 million cells are used for the current study. Table 2 shows the corresponding y+ value on the wall surfaces. The mean and average of the y^+ values are above the boundary layer of the log-law region. This is due to the coarse mesh constructed away from the A-pillar region. However, the current study only focuses on the wind noise generation due to the A-pillar vortex. Thus, to reduce the computational time,

only the mesh near the A-pillar is properly treated. At the A-pillar, the y^+ value is in the range of $3 \leq y^+ \leq 300$. Figure 3 shows the distribution of the y^+ value on the SAE body.

Table 2 The y+ value on the wall

Surface	$\mathbf{y^+_{mean}}$	$\mathbf{y^+_{min}}$	$\mathbf{y^+_{max}}$
Body	337.6	2.68	1180.3
Ground Floor	510.6	22.8	1144.1

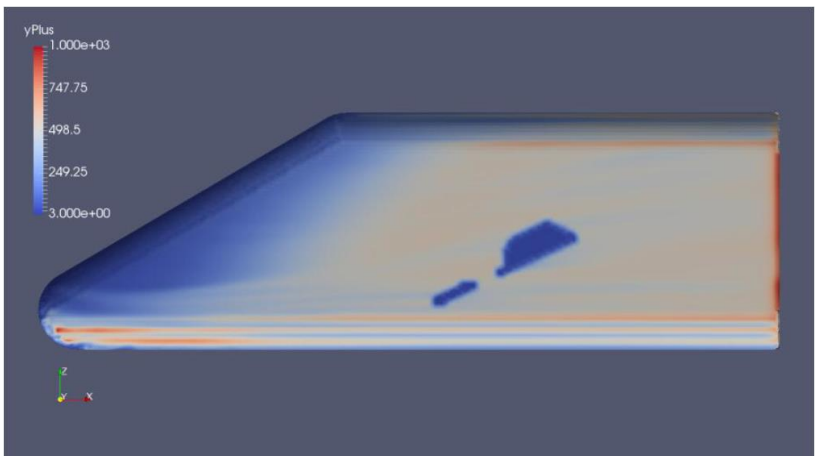

Figure 3 The y^+ distribution on the SAE body

Table 3 The numerical model used for the flow and noise estimations

Property	**Numerical Model**
Turbulent Model	Unsteady Reynolds Averaged Navier Stokes (URANS) based on Menter [7,8]
Convective scheme	2nd-order backward scheme [9]
Time scheme	2nd-order QUICK scheme [10]
Courant-Friedrichs-Lewy (CFL)	Below 0.8 [11]
Acoustic Calculation	Curle's Analogy

Governing Equations and Flow Condition

The numerical model for the flow simulation is set identical to the author previous paper [6]. Table 3 summarized the numerical modelling for the current study.

Acoustic Calculation

The noise source is obtained from the flow simulation where the hydrodynamic pressure fluctuations (*p(t)*) at selected points are measured as shown in Figure 4.

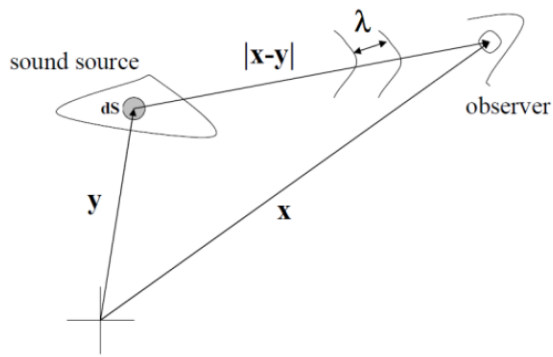

Figure 4 Annotation for the sound propagation

Taking the A-pillar as the focus of the current study, the measurement points are located along the A-pillar. The reasonable number of measurement points is based on the expected sound wavelength (λ), where for the compact sound source assumption used in the Curle acoustic analogy, the sound wavelength must be greater than the length of the sound source (λ >> D). The sound wavelength is estimated by;

$$\lambda = \frac{C_o}{f} \tag{1}$$

where C_o and f are the speed and frequency of the sound, respectively. Thus, for the sound frequency of 2000 Hz the number of measurement points (N) is of at least;

$$
\begin{aligned}
N &\geq \frac{L}{\lambda} \\
&\geq L\frac{f}{C_o} \\
&\geq 1.62\left(\frac{2000}{340}\right) \\
&\geq 10
\end{aligned}
\tag{2}
$$

In the current study, 14 equidistant measurement points along the A-pillar have been made. Table 4 listed the locations of the measurement points from the observer position at a coordinate of (-2.2, 0.8, 0.3).

Table 4 The locations of the microphones relatives to the observer location, i.e., at the centre of the side window glass (-2.2, 0.8, 0.3)

Points	Area	Distance	Direction (degree)
1	0.0135	1.5316	103.3
2	0.0135	1.4707	98.4
3	0.0135	1.3145	99.4
4	0.0135	1.1588	100.7
5	0.0135	1.0039	102.4
6	0.0135	0.8501	104.7
7	0.0135	0.6983	108.0
8	0.0135	0.5489	114.1
9	0.0135	0.4097	123.2
10	0.0135	0.2873	138.7
11	0.0135	0.2258	173.2
12	0.0135	0.2501	30.4
13	0.0135	0.2848	28.6
14	0.0135	0.3700	47.5

Validation

The results obtained from the current calculations are validated with the experimental measurement of Hartmann et al. [3]. The condition chosen is for free stream velocity of 140 km/h and without the side mirror. The validation

involves comparisons of the sound source at the side window and the sound pressure level inside the cabin.

Sound Source

The sound source aerodynamically emitted from the side window is derived from the time gradient of fluctuating hydrodynamic pressure ($\partial p/\partial t$). The numerical calculation is validated with the experimental measurement by Hartmann et al. [3] and it is presented in Figure 5. At $f \leq 6000$ Hz, the numerical result is in agreement with the experiment with only 10 dB different. At $f > 6000$ Hz, the numerical calculation is found not able to predict the sound emission reasonably.

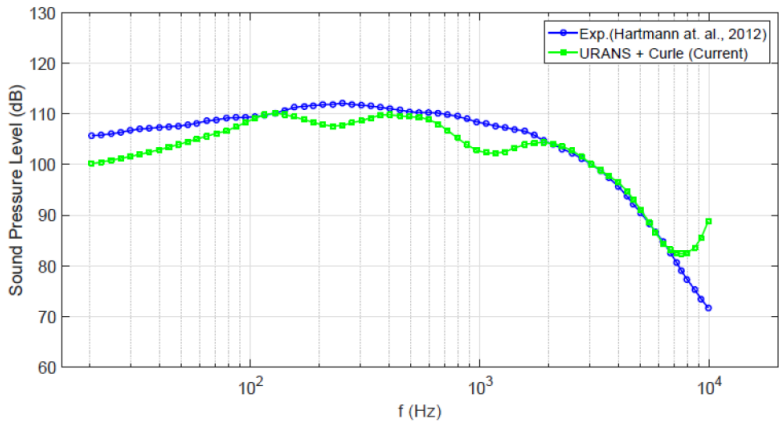

Figure 5 Numerical (current) and experimental [3] results of sound source pressure level on the window glass of SAE type 4 model

Internal Noise

The internal noise is calculated by considering the sound transmission loss (R). In the current study, the sound transmission loss is calculated using the law of frequency [6,12]

Figure 6 compares the internal noise due to the A-pillar noise between the current numerical result and experimental measurements by Hartmann et al. [3]. The A-pillar nise is numerically measured from the 14 measurement points as listed in table 4. Due to the assumption used in the calculation of sound transmission loss, the numerical result only shows a good agreement in the law of frequency region of $132.6 \leq f\,(\text{Hz}) \leq 1971$.

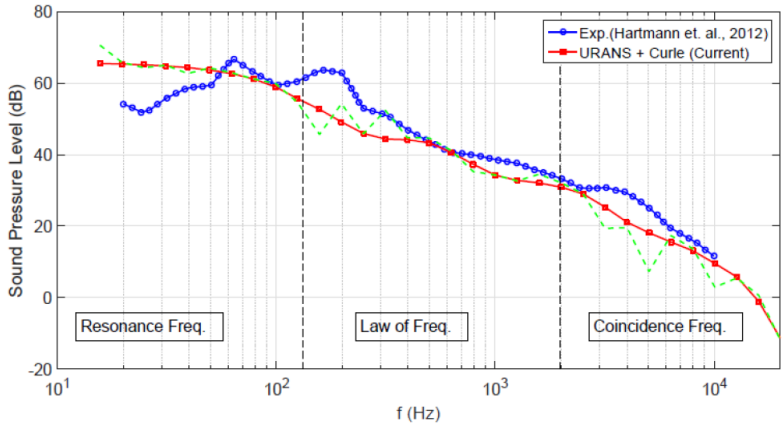

Figure 6 Comparison of SPL inside the cabin between the current simulation and experimental measurement of Hartmann et al. [3]. The smoothed line (red-solid line) is obtained by applying robust local regression with residual of 0.35

Noise Characteristics

The aerodynamic noise that is propagated into the cabin can be controlled efficiently if the characteristic of the noise is understood. This section discusses the characteristics of the noise sources that radiates to an observer position, i.e., near the driver position.

Sound Source Level

Referring to Eqt. 15, the sound source is the time gradient of the hydrodynamic pressure fluctuations ($\partial p/\partial t$). The sound source level (SSL) along the A-pillar is evaluated from its root mean square (rms) of the fluctuating sound source.

$$\mathbf{SSL_i} = 20\log_{10}\left[\frac{\left(\frac{\partial p_i}{\partial t}\right)_{rms}}{20\times10^{-6}}\right] \tag{3}$$

where subscript **i** is the point of measurement. Figure 7 shows the distribution of the sound source level along the A-pillar of the SAE type 4 model.

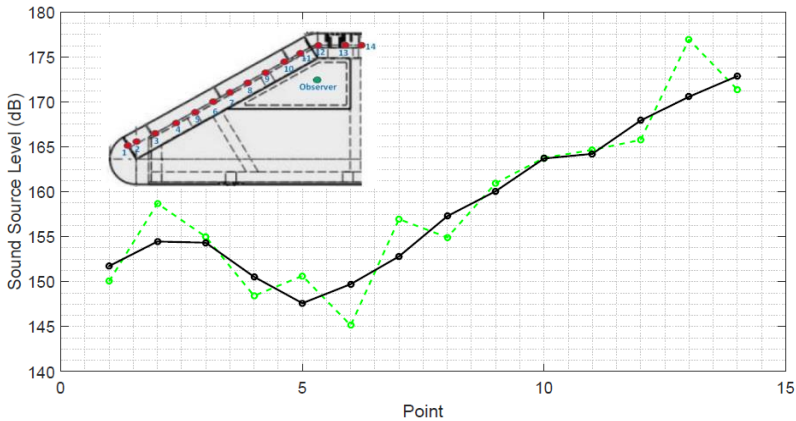

Figure 7 Sound source ($\partial p/\partial t$). level (SSL) on each A-pillar element. The smoothed line (black) is obtained by applying robust local regression with a residual of 0.45. The inset shows the location of the measured noise sources along the A-pillar

Near the root of the A-pillar, the sound source level (SSL) is relatively small if compared to the sound source level near the end of the A-pillar. Downstream of point 5, the SSL almost increases linearly and it reaches an SSL maximum value at the end of the A-pillar. No clear justification can be made at this stage of the study to explain physically on this behaviour. However, it is understood that A-pillar vortex is developed downstream of the A-pillar root and the strength is getting bigger near the end of the A-pillar. Thus, it may suggest that the noise source generation in this region (downstream of point 5) is due to the development of the A-pillar vortex. Future study will investigate this phenomenon in more details.

Sound Pressure Level

The sound source level (SSL) can provide explanations on the generation of the sound source. However, it cannot give the actual sound pressure value at the observer position. The sound pressure level (SPL) at the observer position is not only considering the sound source value but also it takes into account the distance ($R = \mathbf{x} - \mathbf{y}$) and the direction ($\theta$) of the sound to travel. This has been explained in Sec. Acoustic Calculation. Thus, SPL at a specific observer position can identify the contribution from each sound source to the total noise source. Figure 8 shows the distribution of the sound pressure level (SPL) along the A-pillar of the SAE type 4 model. The SPL is calculated as follows;

$$\mathbf{SPL_i} = 20\log_{10}\left[\frac{p'_{rms}}{20\times10^{-6}}\right]_i \tag{4}$$

where the fluctuating sound pressure is calculated from Eq. 15 with the distance and direction for each sound source relative to the observer position is listed in Table 4.

A similar pattern as observed for the SSL distribution is also observed for the SPL distribution. However, almost plateau values are observed near the root (≤ point 5) and near the end (≥ point 11) of the A-pillar. Thus, for SAE type 4 model, the focus should be made on reduction of the sound radiated from the end of the A-pillar, where it contributes to the highest level of noise at the observer position (near the driver).

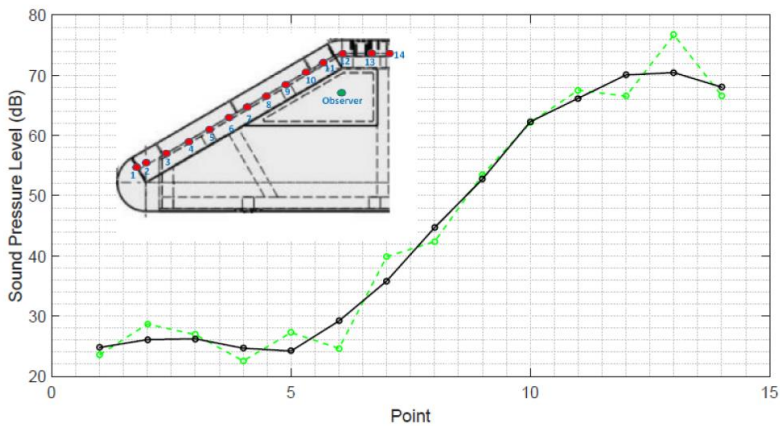

Figure 8 Contribution of internal sound pressure level from each A-pillar segment. The coordinate of the observer position is (-2.2 0.8 0.3). The smoothed line is obtained by applying robust local regression with a residual of 0.45

Fluctuating Sound Pressure

The sound pressure level (SPL) is the statistical value, i.e., rms value, of the fluctuating sound pressure signals. Detailed characteristics of the sound pressure can be observed from the time histories of the sound pressure signals. Figure 9 to 12 show the fluctuating sound pressure (p') at various locations along the A-pillar of the SAE type 4 model. Generally, the maximum value of the sound pressure (p'_{max}) near the root of the A-pillar is one order of magnitude lower than at the middle of the A-pillar. Contrary, the sound pressure near the end of the A-pillar is one order magnitude higher than at the middle. These regimes correspond well with the pattern observed in the change of SPL along the A-pillar as shown in Figure 8 previously.

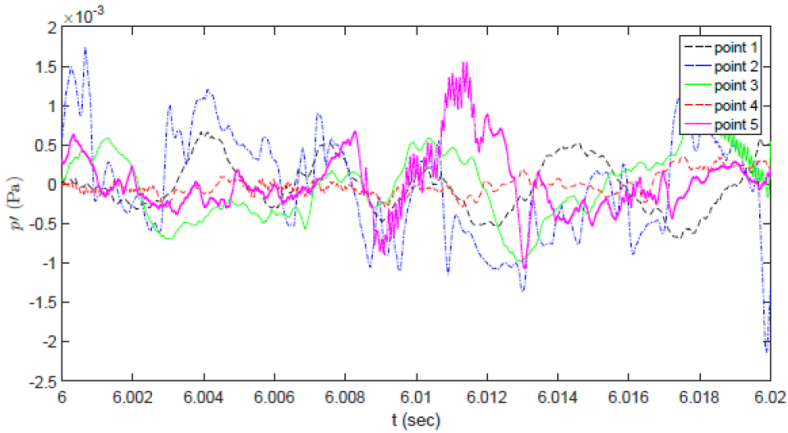

Figure 9 Time histories of fluctuating sound pressure (p') at various locations near the root of A-pillar

At near the root, the fluctuating sound pressure is very severe. No sinusoidal pattern can be observed and the pattern is random. This type of signals is usually associated with flow containing many small eddies. It is postulated that flow separation happens at the front edge of the model. The separation induces eddies of various time and length scales. However, flow visualisation is required to confirm this.

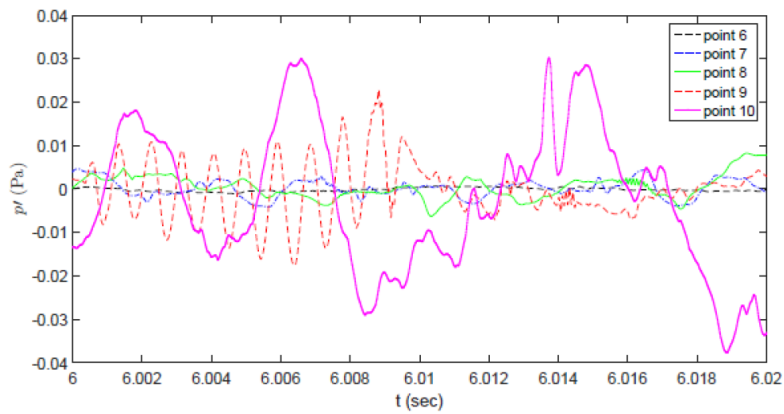

Figure 10 Time histories of fluctuating sound pressure (p') at various locations near the middle of A-pillar

In the middle of the A-pillar, the randomness of the signals is weakening. However, the amplitude fluctuation of the sound pressure is larger than near the root of the A-pillar. It is postulated that at this region, A-pillar vortex is developed. A-pillar vortex is a conical vortex that is dominated by one large eddy. The strength of the vortex is increased as it grows downstream. Thus, it increases the generation of the sound pressure level.

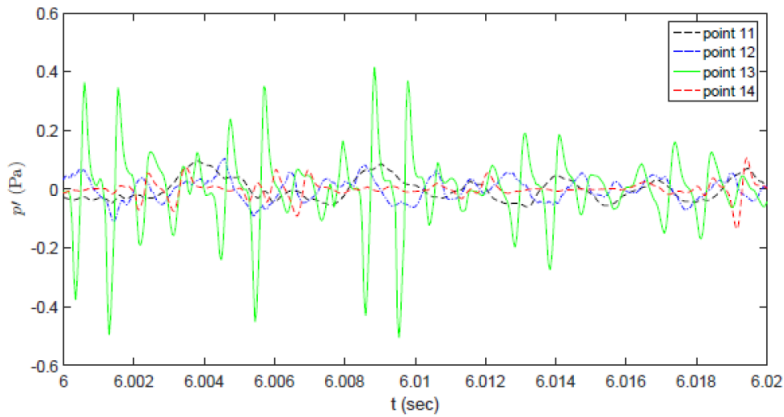

Figure 11 Time histories of fluctuating sound pressure (p') at various locations near the end of A-pillar

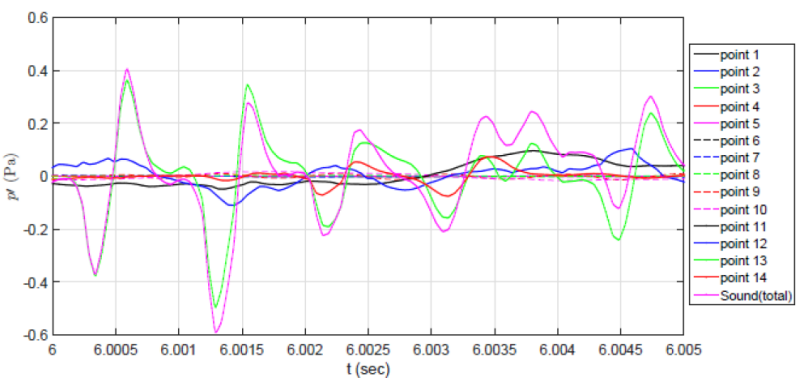

Figure 12 Comparison of fluctuating sound pressure (p') at various locations near the root of A-pillar

A well-defined fluctuating pattern (less signal randomness) is observed near the end of the A-pillar. At this region, it is postulated that the A-pillar vortex is fully formed and start to decrease in its strength at point 13. At this point, the sound pressure dominates the total sound pressure, see Figure 11. Thus, to reduce the total sound pressure at the observer point, the current study

suggests in reducing the sound generation at point 13. This can be made by reducing the interaction of A-pillar vortex with this location or modifying the shape of the A-pillar, particularly at this point so that the sound source can be eliminated or at least be reduced. This is the direction of future study of this project.

Conclusion

The main aim of the current study is to validate the hybrid method used to estimate the sound due to aerodynamic loading. The validation is a comparison study between the current calculations with the sound measurement taken at the AUDI anechoic wind tunnel by Hartmann et al. [3]. The model is a generic SAE type 4 fullback and the sound pressure is measured at the window glass and also inside the cabin. A good agreement between the current study and experimental measurement is obtained at a frequency range $200 < f\ (Hz) < 2000$. At other frequency ranges, the law of frequency used to predict the sound transmission through the glass panel is not able to consider the effect of vibration of the panel. However, the current study able to predict the location of the sound source that dominates the total sound pressure at the observer point (near the driver). This identification is important in an effort to reduce the noise inside the cabin by reducing the noise due to the aerodynamic loading.

References

[1] K. Ono, R.Himeno, & T. Fukushima, "Prediction of wind noise radiated from passenger cars and its evaluation based on auralization," Journal of Wind Engineering and Industrial Aerodynamics 81(1), 403-419 (1999).

[2] W.-H. Hucho, "Aerodynamics of road vehicles: from fluid mechanics to vehicle engineering," *Elsevier* (2013).

[3] M. Hartmann, J.Ocker, T. Lemke, A.Mutzke, V.Schwarz, H. Tokuno, R.Toppinga, P.Unterlechner, & G.Wickern, "Wind noise caused by the A-pillar and the side mirror flow of a generic vehicle model," 18th AIAA/CEAS Aeroacoustic Conference, AIAA paper, (2205), (2012).

[4] M.Islam, F. Decker, M. Hartmann, A. Jaeger, T. Lemke, J. Ocker, V. Schwarz, F. Ullrich, A. Schroder, & A. Heider, "Investigations of sunroof buffeting in an idealised generic vehicle model-part i: Experimental results," 29th AIAA Aeroacoustics Conference, (2900), (2008).

[5] M.Islam, F. Decker, M. Hartmann, A. Jaeger, T. Lemke, J. Ocker, V. Schwarz, F. Ullrich, B. Crouse, G. Balasubramanian, F. Mendonca, "

Investigations of sunroof buffeting in an idealised generic vehicle model-part II: Numerical simulations," 29th AIAA Aeroacoustics Conference, (2008).

[6] M. S. M. Ali, J. Jalasabri, A. M. Sood, S. Mansor, H. Shaharuddin & S. Muhamad, "Wind noise from A-pillar and side view mirror of a realistic generic car model, DrivAer,*"* Int. J. Vehicle Noise and Vibration, 14(1), 38-61 (2018).

[7] F. Menter, M. Kuntz, & R. Langtry, "Ten years of industrial experience with the SST turbulence model, "Turbulence, heat and mass transfer 4(1): 625-632 (2003).

[8] F. R. Menter, "Two-equation eddy-viscosity turbulence models for engineering applications," AIAA Journal, 32(8), 1598-1605 (1994).

[9] H. Jasak, "Error analysis and estimation for the finite volume method with applications to fluid flows, PhD thesis," Department of Mechanical Engineering, Imperial College of Science, Technology and Medicine (1996).

[10] B. P. Leonard, "A stable and accurate convective modelling procedure based on quadratic upstream interpolation," Computer Methods in Applied Mechanics and Engineering 19(1), 59 – 98 (1979).

[11] R. Courant, K. Friedrichs, & H. Lewy, " On the partial differential equations of mathematical physics," IBM journal 11(2), 215-234 (1967)

[12] A. J. Tadeu, & D. M. Mateus, " Sound transmission through single, double and triple glazing, experimental evaluation," Applied Acoustics 62(3), 307-325 (2001).